Research Article

Development of a heat treatment strategy for the γ-TiAl based alloy TNM-B1 to increase the hot workability

Mark Eisentraut[1] · Sebastian Bolz[1] · Irina Sizova[2] · Markus Bambach[2] · Sabine Weiß[1]

Received: 6 August 2019 / Accepted: 22 October 2019 / Published online: 30 October 2019

Abstract
Currently, TiAl turbine blades produced by isothermal forging are commercially used in aircraft jet engines. The limited workability of the HIPed microstructure causes long processing times because of low ram speeds and excessive wear on the costly molybdenum tools due to high forging stresses and temperatures. By introducing a multi-step heat treatment into the industrial forging chain, the formability of the material can be improved, leading to lowered production costs. In this work, the parameters of interest for improved formability are increased β/β_0 phase fractions, increased cellular phase fractions and reduced proportions of lamellar colonies. Several two-step heat treatments were investigated. The parameters of interest were then measured and compared. Subsequently, compression tests were carried out for the most promising heat treatments. It could be shown that a flow stress reduction of around 10% can be achieved by one of these heat treatments (1300 °C/1 h/AC + 1100 °C/5 h/AC). For this heat treatment, reproducibility was also checked using differential scanning calorimetry.

Keywords Titanium aluminide · TNM-B1 · Heat treatment · Hot isothermal forging

1 Introduction

Titanium aluminide (TiAl) alloys based on the ordered γ-TiAl phase have drawn much attention in recent years, due to their great potential in high temperature applications [1, 2]. The main characteristics distinguishing this intermetallic material from other construction materials are high specific yield strength, low density (3.9–4.2 g/cm^3) high corrosion resistance and good creep properties at high temperatures [3–5]. The areas of application includes isothermally forged turbine blades for aircraft engines, as TiAl blades offer reduced weight and similar strength compared to the conventional nickel-based blades [6]. For this purpose, TNM-B1 is one of the most commonly used titanium aluminides with a chemical composition of Ti–(42–45)Al–(3–5)Nb–(0.1–2)Mo–(0.1–0.2)B (in at.%). However, the application possibilities are still limited, mainly due to the difficult production conditions. The limited workability leads to excessive wear of the expensive molybdenum-based tools, which in turn frequently leads to die fractures [7, 8]. As already shown by several studies, a suitable heat treatment can be a first step towards improving hot forming behaviour and microstructural development of titanium aluminides [9–11]. By using an appropriate heat treatment, optimal deformation properties can be achieved, allowing forging at either lower temperatures or higher speeds without damage. In this work, different heat treatments with the aim of improving the deformation behaviour of TNM-B1 have been analyzed and compared.

✉ Mark Eisentraut, Mark.Eisentraut@b-tu.de; Sebastian Bolz, Sebastian.Bolz@b-tu.de; Irina Sizova, Sizova@b-tu.de; Markus Bambach, Bambach@b-tu.de; Sabine Weiß, Sabine.Weiss@b-tu.de | [1]Department of Physical Metallurgy and Materials Technology, Brandenburg University of Technology Cottbus-Senftenberg, Konrad-Wachsmann-Allee 17, 03046 Cottbus, Germany. [2]Chair of Mechanical Design and Manufacturing, Brandenburg University of Technology Cottbus-Senftenberg, Konrad-Wachsmann-Allee 17, 03046 Cottbus, Germany.

2 Materials and methods

The alloy TNM-B1 investigated in this work has a nominal composition of Ti–43.5Al–4Nb–1Mo–0.1B (in at.%). The alloy is a titanium aluminide based on the ordered γ-TiAl phase. It was produced by GfE Metalle und Materialien GmbH (Nürnberg, Germany) using a VAR skull melter and cast by a centrifugal casting process [2, 12]. Afterwards the material was hot isostatically pressed (HIPed) to close the casting porosities using the parameters 1200 °C, 200 MPa and 4 h. The produced ingot had a height of 150 mm and a diameter of 49 mm. Literature reveals that the Al-content has a big influence on the transition temperatures [2]. A modification in Al-content of 0.5 at.% leads to a shift in the γ-solvus temperature of about 30 °C. Table 1 shows the exact composition certified by GfE. A slight deviation in the Al-content of 0.2% with respect to the nominal value can be observed.

In order to find a suitable heat treatment (HT), three slices with a thickness of 10 mm were cut from the original cast and HIPed ingot. To avoid chemical impurities which may arise during production, all slices were cut from the same end of the ingot. Each slice was then cut into several cubes (approximately 10 × 10 × 10 mm). All heat treatments were performed in an industrial furnace from Nabertherm GmbH (Lilienthal, Germany) under atmospheric conditions. The heat treatment schedule is illustrated in Table 2.

The first part of the heat treatment consisted of solution annealing. For this purpose, the temperatures were selected from various fields of the TNM-B1 phase diagram [13, 14]. The first temperature of 1230 °C is below the γ-solvus, the second of 1300 °C between the γ-solvus and the β-transus and the third of 1400 °C above the β-transus. All solution heat treatments were done for 1 h followed by air cooling (AC). Subsequently, the samples were heated once more to annealing temperatures of 900 °C, 1000 °C or 1100 °C for 5 h or 10 h followed by AC. The combination of solution heat treatment at 1400 °C and 10 h annealing time was not considered.

The microstructure of the samples was studied using a TESCAN Mira II XMH (Brno, Czech Republic) scanning electron microscope (SEM). All images were made in backscattered electron (BSE) mode with an acceleration voltage of 15 kV. To ensure adequate image quality the sample surface was ground with a RotoPol-22 from Struers (Berlin, Germany). SiC grinding paper with a gradation ranging from 240 to 2500 was used. After grinding the samples were polished in a mixed solution of distilled water and colloidal silica, from LECO Corporation (St. Joseph, Missouri, USA) by using a VibroMet 2 from Buehler (Uzwil, Switzerland) for 72 h.

Table 2 Considered heat treatment procedures for Ti–43.7Al–4Nb–1Mo–0.1B (in at.%)

Heat treatment	Solution HT [°C]	Sol. HT time [h] (cooling)	Annealing HT [°C]	Ann. HT time [h] (cooling)
X1	1230	1 (AC)	900	5 (AC)
X2			1000	
X3			1100	
X4			900	10 (AC)
X5			1000	
X6			1100	
X7	1300	1 (AC)	900	5 (AC)
X8			1000	
X9			1100	
X10			900	10 (AC)
X11			1000	
X12			1100	
X13	1400	1 (AC)	900	5 (AC)
X14			1000	
X15			1100	

SEM images with an area of 252.8 μm^2 were used for the microstructure analysis. The images were taken in the middle of the samples. For the analysis of the phase content and the grain size, the software Atlas from TESCAN was used. Since only the β/β$_0$ phase can be determined exactly by the optical evaluation, only these values were used for the evaluation. To analyse the lamellar colonies, the lamellar colonies were colored using a single color. Subsequently a software called Gwyddion 2.42 was used to determine the lamellar content.

The phase transition temperatures were verified using high-temperature differential scanning calorimetry (DSC) with the device 404F3 from Netzsch (Selb, Germany) and a heating rate of 40 K/min from RT to 800 °C and 10 K/min from 800 to 1450 °C. The contact surface of samples with 5 mm in diameter and approximately 1 mm in height was made planar by means of grinding. The measurements were conducted in an Ar-atmosphere using a gas flow of 40 ml/min. A temperature accuracy of about ± 5 °C below and ± 7 °C above 1300 °C was obtained. To ensure reproducibility, the experiments were repeated five times for each condition.

The original cast and HIPed ingot (h = 150 mm, Ø = 49 mm) was first cut (h = 95 mm, Ø = 49 mm). Smaller cylinders (h = 95 mm, Ø = 7 mm) were produced from the

Table 1 Chemical composition of alloy TNM-B1 certified by GfE

Element	Ti	Al	Nb	Mo	B	O	Fe
at.%	Bal.	43.7	4.0	1.0	0.1	0.161	0.027

ingot by electrical discharge machining (EDM) by Erocontur GmbH (Müncheberg, Germany). Both the HIPed and the heat treated cylinders were cut and turned into test samples (h = 8 mm, Ø = 5 mm). Subsequently, hot compression tests were performed with a DIL805A/D/T quenching and deformation dilatometer from TA Instruments (New Castle, Delaware, USA) former Bähr Thermoanalyse GmbH. Molybdenum plates with a thickness of around 1 mm were placed between the specimen and the Si_3N_4-punches inside the dilatometer. The tests were conducted in an Ar-atmosphere to protect the samples from oxidation. The cylindrical samples were isothermally deformed at a constant strain rate of 0.01 s^{-1} and 0.001 s^{-1} at the constant temperature of 1150 °C. Samples and molybdenum plates were first heated by induction using a heating rate of 10 K/s, and held at the testing temperature for 3 min to obtain a homogeneous microstructure and quasi-isothermal conditions prior to deformation. Finally, the samples were deformed to a total strain of 0.8 and cooled using argon gas with a cooling rate of 150 K/s. The microstructures after forming have been recorded in the middle of the sample.

3 Results

3.1 Heat treatment study

According to [11], the solidification path from the liquid to the stable solid for alloy TNM-B1 is: $L \rightarrow L + \beta \rightarrow \beta \rightarrow \alpha + \beta \rightarrow \alpha + \beta + \gamma \rightarrow \alpha + \beta + \beta_0 + \gamma \rightarrow \alpha + \beta_0 + \gamma \rightarrow \alpha + \alpha_2 + \beta_0 + \gamma \rightarrow \alpha_2 + \beta_0 + \gamma$. Figure 1a shows the initial material TNM-B1 produced by GfE, which was cast and HIPed. A typical three-phase microstructure can be observed, consisting of γ-TiAl (dark), α_2-Ti_3Al (gray) and β/β_0-TiAl (bright). The fine and homogeneous structure due to the solidification after casting was further refined by the subsequent HIP process. The microstructure includes 57% α_2/γ-colonies, 18% β/β_0 phase, 25% globular γ grains, and is classified as near lamellar [3]. The lamellar colonies mainly consisted of γ-TiAl and α_2-Ti_3Al. Occasionally some β_0-TiAl can be observed within the colonies. This can be attributed to the HIP process, in which α is converted to γ + β. In addition, this can lead to an increase in thickness of the γ-lamellae. Furthermore, it can be assumed that ω-domains are

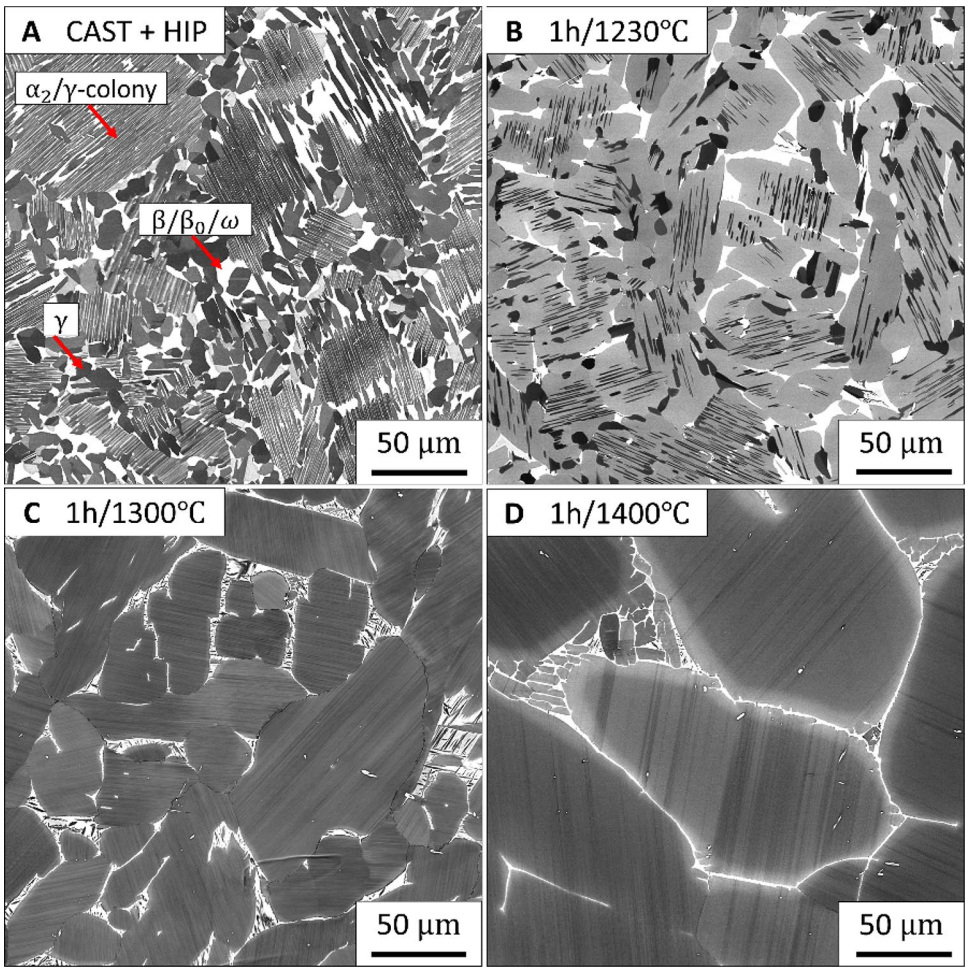

Fig. 1 Microstructure of alloy Ti–43.7Al–4Nb–1Mo–0.1B (in at.%): **a** initial material (cast + HIPed), annealing of 1 h at **b** 1230 °C, **c** 1300 °C and **d** 1400 °C

embedded into the β/β_0 phase [15]. The α_2 phase has a $D0_{19}$ structure and the highest strength and lowest deformability within the TNM-B1 system. The γ phase has a $L1_0$ structure with higher strength than the β/β_0 phase, but higher deformability than the α_2 phase. The β_0 phase has a B2 structure and the disordered β phase a A2 structure. At room temperature the β and the β_0 phases are brittle and exhibits low deformability. However, at hot forging temperatures the both phases become more deformable and are the softest phases in the TNM-B1 system [16]. This occurs in the β phase partly due to sufficient independent slip systems being available at high temperatures [17]. For the β_0 phase however, the Burgers vector is much larger than for the β phase. This causes the β_0 phase to be comparatively less deformable than the β phase. Therefore, the parameter of interest for improved formability is not only the volumetric fraction of β/β_0 phase, but also the dispersion and individual fractions of the two. Also the β/β_0 phase carries a much higher strain during hot deformation than the nominal value, leading to highly misoriented subgrains and dynamic recrystallization (DRX).

To produce a microstructure for TNM-B1 with higher formability than the cast and HIPed one, several two-step heat treatments were considered. The first step of each heat treatment was a solution annealing in three different areas of the phase diagram. For annealing below the γ-solvus 1230 °C ($\alpha+\beta/\beta_0+\gamma$ field), above the γ-solvus 1300 °C ($\alpha+\beta$ field) and 1400 °C ($\alpha+\beta$ field) for the area near the β-transus boundary were chosen.

In the following, the microstructures are compared on the basis of the three parameters that have already been shown to have a positive effect on the forming behavior of TiAl [18, 19]. These parameters are high β/β_0 phase fractions, high cellular phase fractions and low proportions of lamellar colonies.

Figure 1b shows the microstructure of alloy Ti–43.7Al–4Nb–1Mo–0.1B (in at.%) after annealing for 1 h at 1230 °C followed by AC. The microstructure consists of α_2/γ-colonies with a significant amount of α and a few γ platelets with a lamellar content of 91.4%. Between these colonies is a globular structure consisting of β/β_0 phase with a degree of γ grains at the colony boundaries. The proportion of the β/β_0 phase has decreased from 18.0 to 7.4% compared to the cast and HIPed material. Figure 1c displays the microstructure after annealing for 1 h at 1300 °C followed by AC. Compared to Fig. 1b, solution annealing took place in the $\alpha+\beta$ phase region. Since this is above the γ-solvus, the γ content is very low and can be attributed to the cooling process. The microstructure consists of 92.3% lamellae. The β/β_0 content is 5.5%. Figure 1d shows the microstructure of alloy Ti–43.7Al–4Nb–1Mo–0.1B (in at.%) after annealing for 1 h at 1400 °C followed by AC. Similarities to 1c are clearly recognizable, which is due to the fact that both annealing temperatures are above the γ-solvus. Such a solution treatment above the γ-solvus is also known as stabilization treatment [15]. Therefore Fig. 1c and 1d show very fine lamellae within the colonies. The lamellar content of the microstructure presented in Fig. 1d is 96.2% and the average colony size is much larger than in Fig. 1b and c due to the increased solution annealing temperature. The proportion of the β/β_0 phase is 2.9%. Furthermore, no γ platelets can be seen in the β/β_0 phase of Fig. 1d. In contrast, in Fig. 1c the needle-shaped γ platelets are distributed throughout the β/β_0 phase. Thus, the character of the γ platelets seems to be changed. Further research is required for verification. It can be assumed that the platelet formation is considerably limited by the lower β content of the microstructure in Fig. 1d.

Figure 2 displays the microstructures after 5 h for the second heat treatments. The microstructures for the annealing temperatures 900 °C, 1000 °C and 1100 °C are shown from left to right. The different temperatures for the first stage of the heat treatment are shown from top to bottom.

After the second heat treatment, more γ platelets are formed within the α grains, due to the longer heat treatment (Fig. 2a**)**. Within the β/β_0 phase, first parts of the cellular reaction are recognizable, which resembles a disordered accumulation of γ platelets [20]. This reaction starts at the α_2/γ-colony boundaries according to $(\alpha_2+\gamma)_{lam} \rightarrow (\alpha_2+\beta+\gamma)_{cell}$ [11]. A detailed view is shown in Fig. 3a. The γ fraction of the cellular reaction consists of a higher concentration of platelets than the remaining γ fraction within the β_0 phase. The isolated γ platelets form during cooling inside the β/β_0 phase. In addition, globular γ. grains are located at the grain boundaries of the α grains, which precipitate during cooling from the α grains (in 2c from the α_2/γ lamellae). The globular fraction in Fig. 2a is 14.1% and increases with increasing annealing temperature, thus the fraction in Fig. 2c reaches 44.6%. The higher annealing temperature of the microstructure distributed in Fig. 2c has ensured complete formation of the lamellae inside the α grains, resulting in α_2/γ-colonies. Such a microstructure can be defined as duplex one according to [3].

The microstructure distributed in Fig. 2d is similar to the one of 1c. Due to the longer heat treatment in the second step, the average α_2/γ-colony size is decreased. The percentage of colonies is almost identical with 83.2%. The globular content of the γ phase is completely disappeared. Within the β/β_0 phase (5.5%) the percentage of γ platelets is increased (right side of Fig. 3b). In Fig. 2d the cellular reaction can also be observed (left side of Fig. 3b). The γ platelets and the cellular reaction can be distinguished by the strongly different γ content. In condition Fig. 2e these effects are more pronounced. The majority of the microstructure is formed by the cellular structure. There

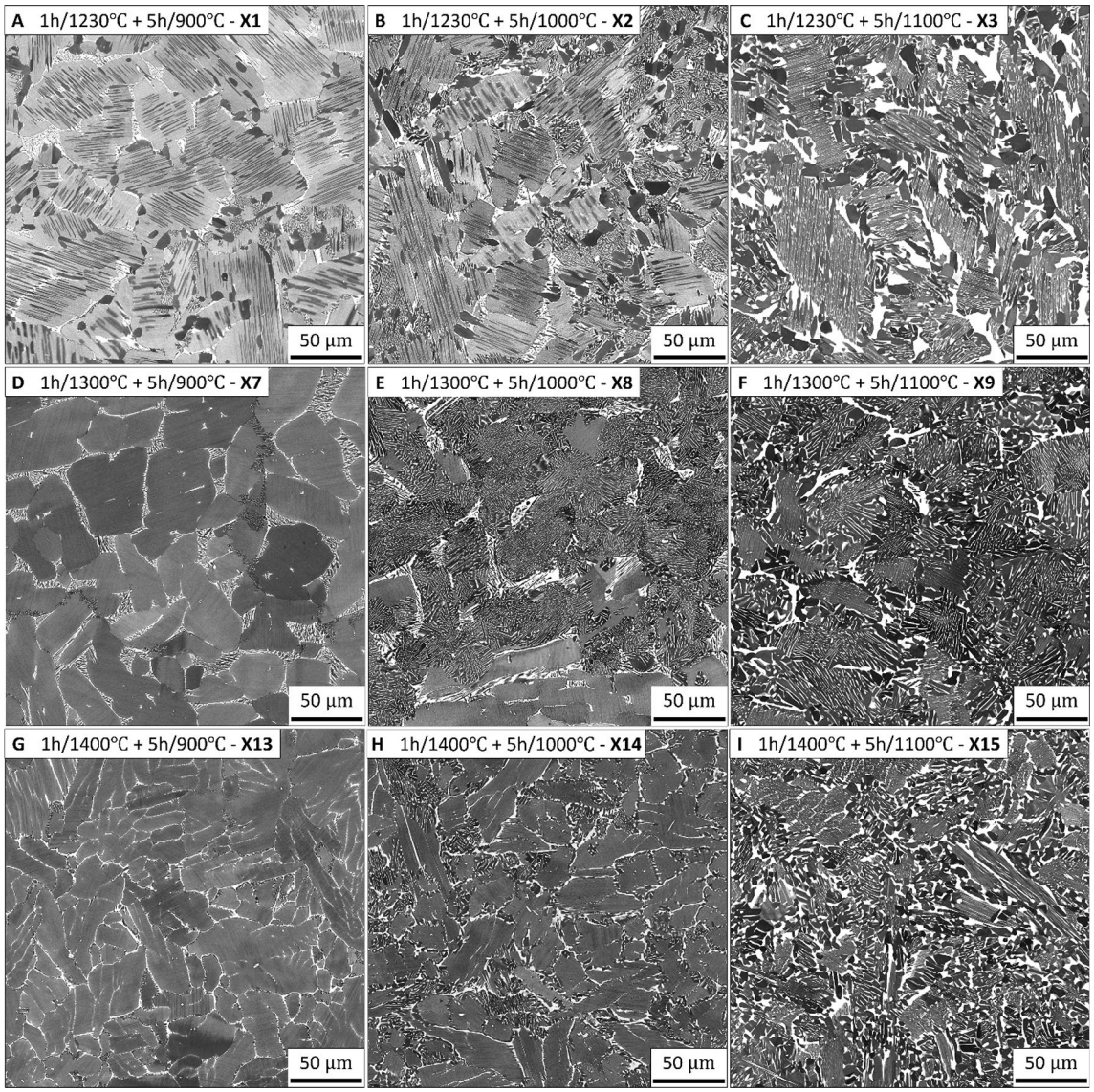

Fig. 2 Microstructure of alloy Ti–43.7Al–4Nb–1Mo–0.1B (in at.%) after both steps of heat treatment: **X1)** 1 h/1230 °C + 5 h/900 °C, **X2)** 1 h/1230 °C + 5 h/1000 °C, **X3)** 1 h/1230 °C + 5 h/1100 °C, **X7)** 1 h/1300 °C + 5 h/900 °C, **X8)** 1 h/1300 °C + 5 h/1000 °C, **X9)** 1 h/1300 °C + 5 h/1100 °C, **X13)** 1 h/1400 °C + 5 h/900 °C, **X14)** 1 h/1400 °C + 5 h/1000 °C, **X15)** 1 h/1400 °C + 5 h/1100 °C

are different preferential directions within the cellular structure. This is shown in detail in Fig. 3c. Furthermore, the β/β_0 content within the microstructure of Fig. 2e is increased to 14.0% and the lamella content is decreased to 17.7%. In the microstructure of Fig. 2f the lamella content drops to 10.4%. In addition, the thickness of the lamellas is increased. Within the cellular structure, the distance between the γ platelets and the lens shaped β/β_0 portion are increased as well. The β/β_0 content remains nearly identical to the one in Fig. 2e with 21.2%.

Figure 2g shows a nearly lamellar structure [3]. Compared to Fig. 1d, the colony size is decreased. The percentage of lamella colonies (84.4%) does not differ from the ones in Fig. 2a and d. Furthermore, the β/β_0 content is with 4.5% the lowest of the tested heat treatments. This is probably a result of secondary heat treatments with an annealing temperature of 900 °C, and should be considered for future research. At many α_2/γ-colony boundaries a weak approach of the cellular reaction can be recognized. In the microstructure Fig. 2h, the β/β_0 content rises to 8.1%. At the same time, the lamellar portion decreases to 59.5%. This value is closer to the value in Fig. 2b than to the value in Fig. 2e. Thus, the content of the structure due to cellular reaction is significantly lower in Fig. 2h than in both Fig. 2e and i. Despite the higher β/β_0 content of 18.9%, the proportion of lamella

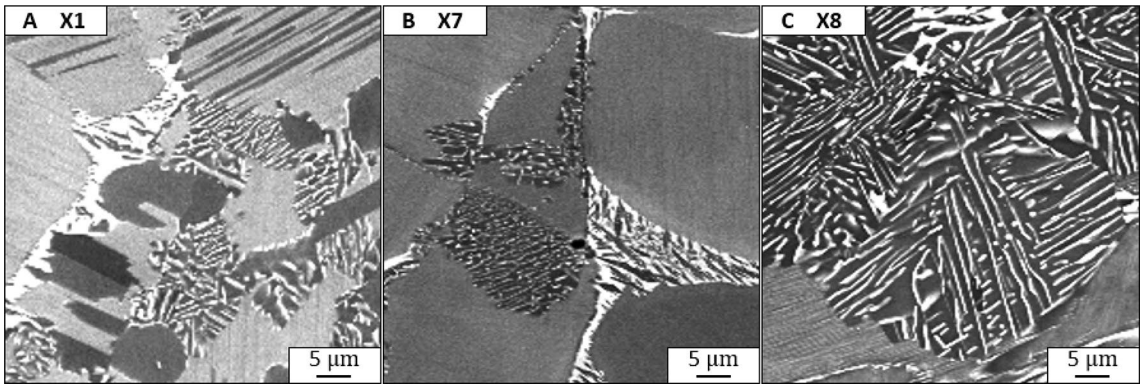

Fig. 3 Characteristics of the cellular reaction in Ti–43.7Al–4Nb–1Mo–0.1B (in at.%) after heat treatment: **X1)** 1 h/1230 °C + 5 h/900 °C, **X7)** 1 h/1300 °C + 5 h/900 °C, **X8)** 1 h/1300 °C + 5 h/1000 °C

colonies (29.1%) is considerably higher than after the heat treatment with lower temperature in the first stage (Fig. 2f). However, cooling from the β region (1400 °C) results in a higher grain refinement compared to cooling from 1230 and 1300 °C. Table 3 shows the values determined for all heat treatments under consideration.

In general, it can be observed that the proportion of lamella colonies is lowest after solution annealing at 1300 °C (X7, X8, X9). At the same time, the cellular content is highest. On the other hand, the β/β_0 content is further increased with increasing annealing temperature. The heat treatment X9 (1 h/1300 °C + 5 h/1100 °C) (ref. Table 2) leads to a microstructure suitable for hot forming, as it has the comparatively lowest lamella content and a relatively high β/β_0 content. In addition, the content of the resulting structure due to the cellular reaction is the highest compared to the other heat treatments.

The microstructures after heat treatments X5–X6 and X10–X12 (ref. Table 2) are not explained in detail as the results hardly differ from those with 5 h annealing time. With regard to a potential industrial application of the final heat treatment, all treatments with a solution temperature of 1400 °C (X13, X14, X15) were excluded from further investigations. It can be assumed that this temperature is too high to achieve an economic benefit. Furthermore, the heat treatment routes X2 and X8 were excluded because results between X1 and X3 as well as X7 and X9 can be assumed. Thus, the four heat treatments X1, X3, X7 and X9 were selected for further investigation.

3.2 Hot-compression tests

In this investigation, the constant forming temperature of 1150 °C was purposely chosen to be below the industrial forging window for cast and HIPed TNM-B1 (1230 to 1250 °C). This was done in order to better assess and compare the deformation and damage behaviors of the heat treated material states, as the differences are expected to be more pronounced at this lower temperature. Furthermore, this was done to assess if the industrial forging window could be expanded to include 1150 °C using one of the studied heat treatments. The measured flow curves from the hot-compression tests for (a) T = 1150 °C/ $\dot{\varepsilon} = 0.01\text{s}^{-1}$ and (b) T = 1150 °C/ $\dot{\varepsilon} = 0.001\text{s}^{-1}$ are depicted in Fig. 4. The samples were deformed to a strain of 0.8. The maximum flow stress decreased with decreasing strain rate. All flow curves show a pronounced stress peak at strains between 0.02 and 0.04 before decreasing due to softening. The initial sharp increase in flow stress can be attributed to work hardening caused by rapid dislocation multiplication [21]. When the defect density reaches a critical value, dynamic recrystallization (DRX) begins, at the so-called critical strain. In general, the flow behavior of the material is governed by the competition of work hardening and work softening due to dynamic recovery (DRV) [22], phase rotation [23], deformation twinning [24], and platelet bending/kinking [25]. The peak stress marks where the hardening and softening processes are in balance. The peak stress values of the cast and HIPed material are (a) 164.5 MPa for $\dot{\varepsilon} = 0.01\text{s}^{-1}$ and (b) 80.2 MPa for $\dot{\varepsilon} = 0.001\text{s}^{-1}$. After the heat treatment X3 these values change to (a) 151.7 MPa and (b) 77.3 MPa, respectively. The

Table 3 Overview of the β/β_0 and the lamellar content (in vol.%) in the air-cooled heat treated samples

HT	X1	X2	X3	X7	X8	X9	X13	X14	X15
β/β_0	11.3	20.3	23.2	5.5	14.0	21.2	4.5	8.1	18.9
Lamellar	85.9	50.6	55.4	83.2	17.7	10.4	84.4	59.5	29.1

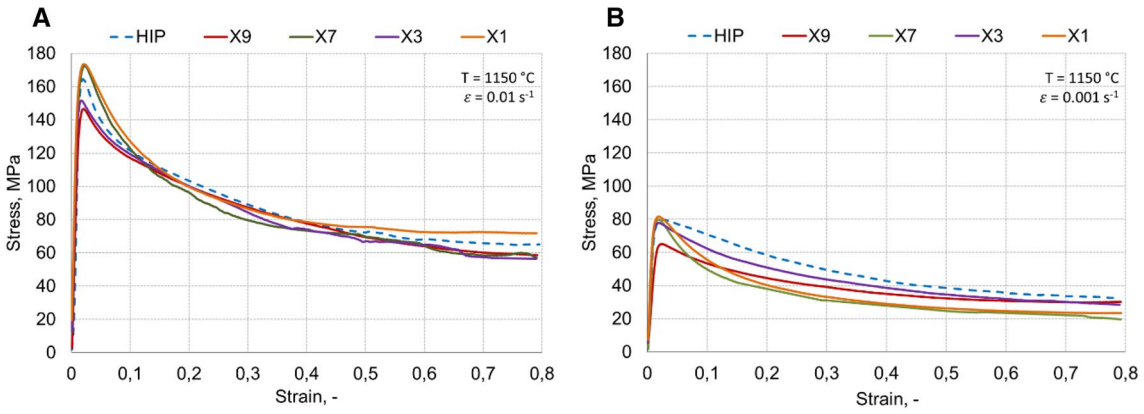

Fig. 4 Flow curves of alloy Ti–43.7Al–4Nb–1Mo–0.1B (in at.%) at **a** T = 1150 °C/ $\dot{\varepsilon} = 0.01 s^{-1}$ and **b** T = 1150 °C/ $\dot{\varepsilon} = 0.001 s^{-1}$: starting material (cast + HIP), **X1**) 1 h/1230 °C + 5 h/900 °C, **X3**) 1 h/1230 °C + 5 h/1100 °C, **X7**) 1 h/1300 °C + 5 h/900 °C, **X9**) 1 h/1300 °C + 5 h/1100 °C

Table 4 Phase transition temperatures [°C] of Ti–43.7Al–4Nb–1Mo–0.1B determined by means of DSC

	T_{eu}	T_{β_0}	$T_{\gamma solv}$	T_{β}
HIP	1175.1 ± 5	1215.7 ± 5	1247.6 ± 5	1423.5 ± 7
X9	1179.6 ± 5	1216.9 ± 5	1241.6 ± 5	1422.5 ± 7

values for the peak stress after heat treatment X9 are the lowest for both deformation velocities with (a) 146.6 MPa and (b) 64.4 MPa, respectively. This results in a peak stress reduction of more than 10% for heat treatment X9 compared to the cast and HIPed, at the tested conditions.

3.3 Dynamic differential calorimetry

In order to ensure the operational capability of heat treatment X9, DSC measurements of the samples processed using heat treatment X9 and the cast and HIPed material were carried out. Table 4 displays the eutectoid temperature T_{eu}, the $\beta_0 \rightarrow \beta$ transition temperature T_{β_0}, the γ-solvus temperature $T_{\gamma solv}$ and the β-transus temperature T_{β}. The values represent the average value of 5 measurements. The results correlate well with the phase transition temperatures measured for the cast and HIPed samples.

Subsequently, the reproducibility of heat treatment X9 was assessed. For this purpose, heat treatment X9 was independently performed four times Each sample was examined by means of SEM. The results are shown in Table 5. There was only one deviation in the measurement of the lamellar portion. Measurement 3 showed a lamellar proportion of 17.4%. This is slightly higher compared to the other measurements.

4 Conclusions

A set of two-step heat treatments was developed, and the resulting microstructures were analyzed with the aim of improving the hot workability of TNM-B1. For this purpose, three solution annealing temperatures (1230 °C, 1300 °C and 1400 °C) and three annealing temperatures (900 °C, 1000 °C and 1100 °C) were chosen. For the annealing temperatures, two different processing times (5 h and 10 h) were considered. However, no significant difference between the two could be observed. Therefore, 5 h was chosen for this investigation. The combination of 1 h/1300 °C + 5 h/1100 °C was shown to be the most suitable due to the resulting high cellular reaction fraction, the high β/β_0 fraction and the low amount of lamellar colonies,

Table 5 Microstructure parameters of all separately performed heat treatments according to X9

	# HT	Phase fraction	Grain size			α_2/γ colony size	
		β	min. d [µm]	max. d [µm]	Ø d [µm]	#	lam. vol.%
X9	1	21.2	2.7	12.4	4.99	16	10.4
	2	26.3	2.5	11.9	5.61	14	13.0
	3	25.1	2.7	15.0	5.03	25	17.4
	4	23.4	3.6	13.5	6.05	20	10.2
	5	23.5	2.7	13.6	5.03	20	13.1
	Ø	23.9	2.84	13.28	5.32	19	12.82

leading to beneficial deformation behavior. Hot compression tests at the temperature 1150 °C and the strain rates 0.01 s^{-1} and 0.001 s^{-1} to a total strain of 0.8 were conducted. The heat treatments X9 (1 h/1300 °C + 5 h/1100 °C) and X3 (1 h/1230 °C + 5 h/1100 °C) resulted in about 10% lower flow stress, when compared with the cast and HIPed material. Finally, DSC measurements showed no large deviations in phase transition temperatures for the heat treatment X9.

Acknowledgements This research has been funded by the Deutsche Forschungsgemeinschaft (DFG, German Research Foundation) through the projects WE 2671/7-1 and BA 4253/4-1.

Author contributions M. Eisentraut and S. Bolz conceived and designed the experiments; M. Eisentraut, S. Bolz and I. Sizova performed the experiments; M. Eisentraut did the SEM investigations; M. Eisentraut wrote the paper; S. Weiß and M. Bambach directed the work and revised the manuscript.

Complaince with ethical standards

Conflict of interest On behalf of all authors, the corresponding author states that there is no conflict of interest.

References

1. Kim Y-W (1994) Ordered intermetallic alloys, part III: gamma titanium aluminides. JOM 46:30–39
2. Clemens H, Mayer S (2013) Design, processing, microstructure, properties, and applications of advanced intermetallic TiAl alloys. Adv Eng Mater 15:191–215
3. Appel F, Paul J, Oehring M (eds) (2011) Gamma titanium aluminide alloys. Wiley, New York
4. Hu D, Godfrey A, Blenkinsop PA, Loretto MH (1998) Processing-property-microstructure relationships in TiAl-based alloys. Metall Mat Trans A 29:919–925
5. Brotzu A, Felli F, Marra F, Pilone D, Pulci G (2018) Mechanical properties of a TiAl-based alloy at room and high temperatures. Mater Sci Technol 34:1847–1853
6. Clemens H, Smarsly W (2011) Light-weight intermetallic titanium aluminides - status of research and development. AMR 278:551–556
7. Lange K (1997) Modern metal forming technology for industrial production. J Mater Process Technol 71:2–13
8. Abachi S, Akkök M, İlhan Gökler M (2010) Wear analysis of hot forging dies. Tribol Int 43:467–473
9. Güther V, Rothe C, Winter S, Clemens H (2010) Metallurgy, microstructure and properties of intermetallic TiAl ingots. BHM Berg Huettenmaenn Monatsh 155:325–329
10. Appel F, Brossmann U, Christopf U, Eggert S, Janschek P, Lorenz U, Müllauer J, Oehring M, Paul JDH (2000) Recent progress in the development of gamma titanium aluminide alloys. Adv Eng Mater 2:699–720
11. Schwaighofer E, Clemens H, Mayer S, Lindemann J, Klose J, Smarsly W, Güther V (2014) Microstructural design and mechanical properties of a cast and heat-treated intermetallic multi-phase γ-TiAl based alloy. Intermetallics 44:128–140
12. Achtermann M, Fürwitt W, Guether V (2011) Method for producing a γ-TiAl base alloy: patent EP2010/064306
13. Schwaighofer E, Schloffer M, Schmoelzer T, Mayer S, Lindemann J, Guether V, Klose J et al (2012) Influence of heat treatments on the microstructure of a multi-phase titanium aluminide alloy. Pract Metallogr 49:124–137
14. Chladil HF, Clemens H, Zickler GA, Takeyama M, Kozeschnik E, Bartels A, Buslaps T et al (2007) Experimental studies and thermodynamic simulation of phase transformations in high Nb containing γ-TiAl based alloys. IJMR 98:1131–1137
15. Wallgram W, Schmoelzer T, Cha L, Das G, Güther V, Clemens H (2009) Technology and mechanical properties of advanced γ-TiAl based alloys. IJMR 100:1021–1030
16. Liu B, Liu Y, Qiu C, Zhou C, Li J, Li H, He Y (2015) Design of low-cost titanium aluminide intermetallics. J Alloy Compd 640:298–304
17. Grujicic M, Zhang Y (1999) Crystal plasticity analysis of the effect of dispersed β-phase on deformation and fracture of lamellar γ + α2 titanium aluminide. Mater Sci Eng A 265:285–300
18. Cao R, Li L, Chen JH, Zhang J, He H (2010) Study on compression deformation, damage and fracture behavior of TiAl alloys. Mater Sci Eng A 527:2455–2467
19. Kim JH, Ha TK, Chang YW, Lee CS (2003) High-temperature deformation behavior of a gamma TiAl alloy—microstructural evolution and mechanisms. Metall Mater Trans A 34:2165–2176
20. Aaronson HI, Enomoto M, Lee JK (2010) Mechanisms of diffusional phase transformations in metals and alloys. Taylor and Francis, Hoboken
21. Yan J, Pan QL, Li B, Huang ZQ, Liu ZM, Yin ZM (2015) Research on the hot deformation behavior of Al–6.2Zn–0.70Mg–0.3Mn–0.17Zr alloy using processing map. J Alloys Compd 632:549–557
22. Yang J, Wang G, Jiao X, Li X, Yang C (2017) Hot deformation behavior and microstructural evolution of Ti 22Al 25Nb 1.0B alloy prepared by elemental powder metallurgy. Journal of Alloys and Compounds 695:1038–1044
23. Han Y, Zeng W, Qi Y, Zhao Y (2011) The influence of thermomechanical processing on microstructural evolution of Ti600 titanium alloy. Mater Sci Eng A 528:8410–8416
24. Wei D-X, Koizumi Y, Nagasako M, Chiba A (2017) Refinement of lamellar structures in Ti-Al alloy. Acta Mater 125:81–97
25. Park CH, Kim JH, Hyun Y-T, Yeom J-T, Reddy NS (2014) The origins of flow softening during high-temperature deformation of a Ti–6Al–4V alloy with a lamellar microstructure. J Alloy Compd 582:126–129